Gunwale bobbing

Graham P. Benham [1,*] Olivier Devauchelle,[2] Stephen W. Morris [3]
and Jerome A. Neufeld [4,5,6]

[1]*Mathematical Institute, University of Oxford, Oxford OX2 6GG, United Kingdom*
[2]*Université de Paris, Institut de Physique du Globe de Paris, CNRS, F-75005 Paris, France*
[3]*Department of Physics, University of Toronto, Toronto, Ontario, Canada M5S 1A7*
[4]*Department of Earth Sciences, University of Cambridge, Cambridge CB3 0EZ, United Kingdom*
[5]*Centre for Environmental and Industrial Flows, University of Cambridge,
Cambridge CB3 0EZ, United Kingdom*
[6]*Department of Applied Mathematics and Theoretical Physics, University of Cambridge,
Cambridge CB3 0WA, United Kingdom*

We investigate gunwale bobbing, a phenomenon in which a person jumping on the
gunwales of a canoe achieves horizontal propulsion by forcing it with vertical oscillations.
The canoe moves forward by surfing the resulting wave field. After an initial transient, the
canoe achieves a cruising velocity which satisfies a balance between the thrust generated
from pushing downwards into the surface gradients of the wave field and the resistance due
to a combination of profile drag and wave drag. By superposing the linear wave theories
of Havelock [Proc. R. Soc. A **95**, 354 (1919)] for steady cruising and Helmholtz for an
oscillating source, we demonstrate that such a balance can be sustained. We calculate the
optimal parameter values to achieve maximum canoe velocity. We compare our theoretical
result to accelerometer data taken from an enthusiastic gunwale bobber and to estimates
from videos of other canoeing aficionados. Finally, we discuss the similarities and differ-
ences with other examples of macroscopic wave-driven bodies and comment on possible
applications to competitive sports.

I. INTRODUCTION

A canoe, or any small boat, can be propelled forward by standing on its gunwales near one
end and forcing vertical oscillations by jumping up and down. This technique, known as gunwale[1]
bobbing, is well known to canoeists but has so far not been described hydrodynamically. We propose
that the thrust sufficient to overcome drag is the result of repeatedly pushing into the surface
gradients of the wave field generated by the forced oscillation itself. In addition to solving an
interesting nonlinear dynamics problem that connects canoeing with wave-driven particles [1], an
understanding of gunwale bobbing may find practical application in the general science of water
sports. In rowing, for example, it is not known how the rhythmic motion of the athletes' bodies
during each stroke contributes to the speed or efficiency.

We apply linear wave theory to a slender, oscillating canoe shape to determine the forcing that
maximizes the cruising speed. The efforts of the canoeist are assumed to produce both pitching (fore
and aft) and heaving (vertical) periodic motions. A simple model for the wave field is derived by

---

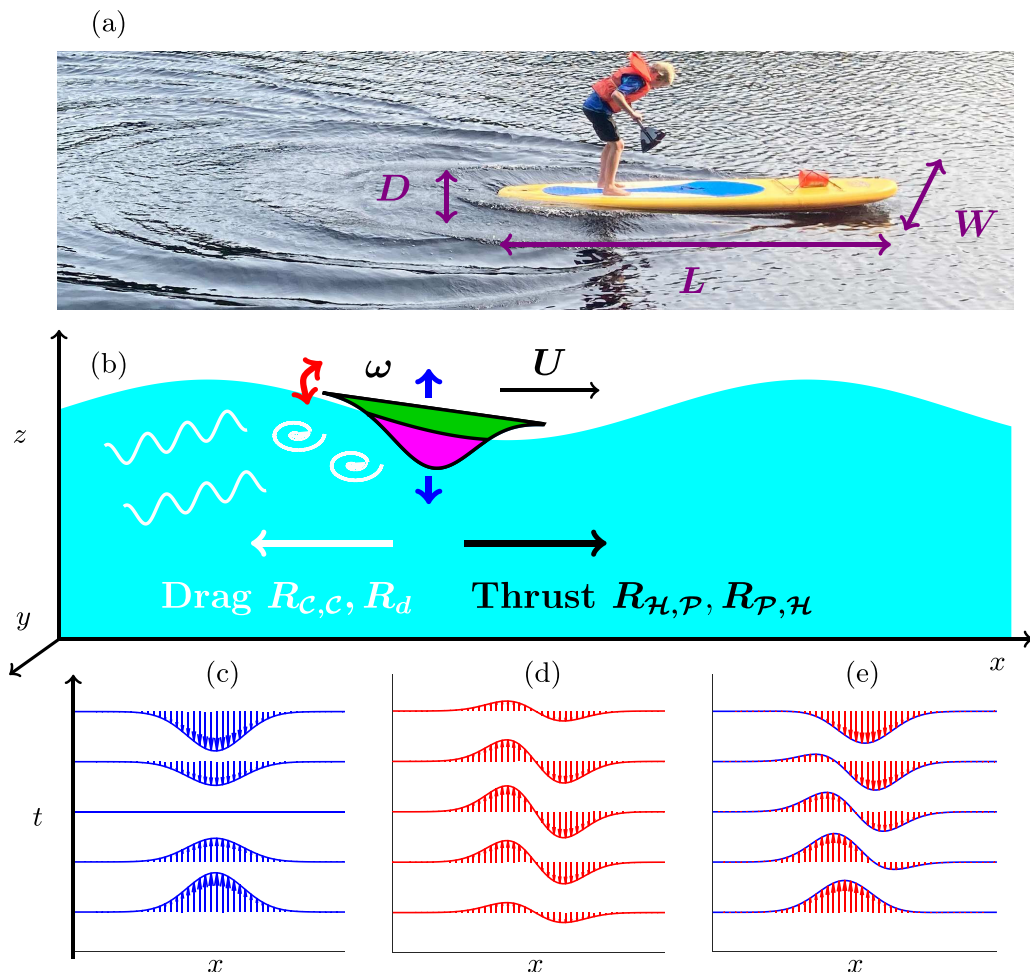[1]The word *gunwale* is pronounced like *gunnel*.

FIG. 1. (a) Gunwale bobbing in action, illustrating the length L, width W, and draft D of the boat (here a paddle board). (b) Illustration of the thrust and drag forces at play. Thrust originates from pushing into surface gradients producing pitching and heaving forces, $R_{\mathcal{H},\mathcal{P}}$, $R_{\mathcal{P},\mathcal{H}}$, at frequency ω, causing the boat to "surf" on its own wave at cruising speed U. Drag originates from wave energy radiation (wave drag, $R_{\mathcal{C},\mathcal{C}}$), skin friction, and vortex separation (profile drag, R_d). (c)–(e) Pressure source term (horizontal slice) in the case of heaving motion in Eq. (4), pitching motion in Eq. (5), and heaving-pitching motion in equal proportion ($\phi = 1/2$) and out of phase ($\theta = \pi/2$).

adapting recent theories of bouncing droplets [2,3]. We demonstrate that certain combinations of pitching and heaving produce a positive thrust force; the canoe "surfs its own waves" (see Ref. [4]). We balance this positive thrust against negative resistive forces due to wave and profile drag to find the steady cruising speed. For typical canoe parameters, we find that ∼1 m/s cruising speeds can be achieved, in broad agreement with observations.

II. HEAVE, PITCH, CRUISE YOUR BOAT, GENTLY DOWN THE STREAM

Consider the wave field generated by a canoe of length L, width W, and draft D, moving at the surface of an infinite body of water, as illustrated in Figs. 1(a) and 1(b). We take the water to be

irrotational and inviscid, with density ρ. From the cruising speed U and oscillating frequency ω, we can define two Froude numbers,

$$\text{Fr} = U/\sqrt{gL}, \quad \text{Fr}_\omega = \omega^{-1}\sqrt{g/L}. \tag{1}$$

The former is used in marine hydrodynamics to quantify the ratio between the length of the wave generated due to cruising and the boat length, and we introduce the latter by analogy for the waves due to an oscillating canoe. We further define two aspect ratios $\alpha = L/W$ and $\beta = L/D$, both of which are large for slender canoes [5]. Henceforth, all variables are given in dimensionless form, with lengths scaled by L, forces scaled by $\rho U^2 L^2$, pressures scaled by $\rho g L$, and time scaled by $\sqrt{L/g}$. Following previous work [5–7], we assume a simplified canoe shape given by a Gaussian:

$$f(x, y) = \exp\left(-x^2/2 - \alpha^2 y^2/2\right). \tag{2}$$

Our goal is to describe the motion resulting from the simultaneous heaving, pitching, and cruising of the canoe, as illustrated in Figs. 1(c)–1(e). Since we restrict our attention to small-amplitude perturbations, we can treat the waves due to each motion separately. The case of pure cruising at constant speed U was addressed by Havelock [8]. The hull's motion is treated as a translating pressure source applied to the water surface

$$p_\mathcal{C} = \delta\beta^{-1} f(x - \text{Fr}\,t, y), \tag{3}$$

with an empirically determined constant amplitude, δ. We use $\delta = 0.4$, a value that was fitted against experimental data [9]. To model the pressure sources for the heaving and pitching motion, we generalize (3) by assuming

$$p_\mathcal{H} = \text{Im}\left\{p_\mathcal{C} \exp\left[i\text{Fr}_\omega^{-1}t\right]\right\} \quad \text{(heaving)}, \tag{4}$$

$$p_\mathcal{P} = \text{Im}\left\{p_\mathcal{C}(x - \text{Fr}\,t) \exp\left[i\left(\text{Fr}_\omega^{-1}t + \theta\right)\right]\right\} \quad \text{(pitching)}, \tag{5}$$

where θ is the phase difference between heave and pitch. For small-amplitude perturbations, it suffices to take the forcing to be a linear combination,

$$p = p_\mathcal{C} + \phi\, p_\mathcal{P} + (1 - \phi)p_\mathcal{H}, \tag{6}$$

where $\phi \in [0, 1]$ is the heave-pitch ratio. Hence, the total wave-field height resulting from this pressure disturbance (6) may be split into a superposition of the corresponding wave-field components $h = h_\mathcal{C} + \phi h_\mathcal{P} + (1 - \phi)h_\mathcal{H}$.

The wave drag due to the cruising disturbance (3) is calculated by noting that the pressure is applied in the manner of a rigid lid fitted to the water surface [6,8]. The wave drag is given by the pressure resolved in the x direction, such that the resistive force for cruising is

$$R_{\mathcal{C},\mathcal{C}} = \frac{1}{\text{Fr}^2} \iint_{-\infty}^{+\infty} p_\mathcal{C} \frac{\partial h_\mathcal{C}}{\partial X}\, dX\, dy, \tag{7}$$

where $X = x - \text{Fr}\,t$ is the horizontal coordinate in the reference frame of the cruising canoe.

By analogy, we may assume that forces similar to the wave drag (7) arise from the interaction between the different pressures and wave fields due to heaving, pitching, and cruising. We represent these forces, averaged over one period $T = 2\pi\text{Fr}_\omega$, as

$$R_{n,m} = \frac{1}{\text{Fr}^2 T} \int_0^T \left(\iint_{-\infty}^{+\infty} p_n \frac{\partial h_m}{\partial X}\, dX\, dy\right) dt, \tag{8}$$

where subscripts n and m correspond to cruising $\mathcal{C}$, heaving $\mathcal{H}$, or pitching $\mathcal{P}$.

Two initial observations can be made. First, the interactions between oscillating and steady terms, such as $R_{\mathcal{C},\mathcal{H}}$, vanish. Second, when the canoe cruises at a moderate velocity, we expect that heaving will generate a fore-aft symmetric wave field, whereas pitching will generate an antisymmetric wave field. In both cases, then, the in-phase interaction $R_{n,n}$ is small. The dominant force terms are thus

those that combine out-of-phase heaving and pitching, which read $\phi(1 - \phi)(R_{\mathcal{H},\mathcal{P}} + R_{\mathcal{P},\mathcal{H}})$. It is immediately clear that $\phi = 1/2$ is the heave-pitch ratio that gives the largest force values. As for the phase lag θ, intuition suggests that $\theta = \pi/2$ is best (numerical simulations, Sec. III B, will confirm this). Hereafter, unless stated otherwise, we fix ϕ and θ to these values, and we set the aspect ratios of the canoe to those used in our best-controlled experiment, $\alpha = 5$, $\beta = 31$ (see Sec. IV).

In addition to the forces due to waves $R_{n,m}$, we must also account for the hydrodynamic forces due to skin friction (viscous stress applied by the water at the wetted surface area) and vortex separation (turbulent eddies in the wake behind the boat that induce low pressures and consequent drag). Known together as *profile drag* R_d, these forces play a dominant role in opposing boat motion (when the cruising Froude number is small) [5]. The profile drag R_d is modeled using a drag coefficient C_d, with

$$R_d = -\tfrac{1}{2}\mathcal{S}(\alpha, \beta)C_d(\alpha, \mathrm{Re}), \tag{9}$$

where $\mathcal{S}$ is the dimensionless wetted surface area and Re is the Reynolds number. We cannot estimate the surface area $\mathcal{S}$ for a Gaussian hull (it would be infinite). Instead, we have approximated the surface area by taking the canoe shape as the sum of two tetrahedrons. Expressions for $\mathcal{S}$ and the drag coefficient C_d (approximated using empirical formulas [5,10,11]) are given in Appendixes C and E.

For small-amplitude perturbations, the total horizontal force is the sum of the individual components

$$R_H = \phi^2 R_{\mathcal{P},\mathcal{P}} + (1 - \phi)^2 R_{\mathcal{H},\mathcal{H}} + \phi(1 - \phi)(R_{\mathcal{H},\mathcal{P}} + R_{\mathcal{P},\mathcal{H}}) + R_{\mathcal{C},\mathcal{C}} + R_d, \tag{10}$$

as is commonly found in other boating problems [5,12]. The cruising speed is determined by solving the nonlinear force balance

$$R_H(\mathrm{Fr}; \mathrm{Fr}_\omega, \alpha, \beta, \phi, \theta) = 0, \tag{11}$$

for Fr, where the remaining parameters $\mathrm{Fr}_\omega, \alpha, \beta, \phi, \theta$ are fixed by the bobber and the boat.

III. WAVE-FIELD AND FORCE CALCULATIONS

A. Waves due to cruising

Expressions for the wave-field height $h_{\mathcal{C}}$ and wave resistance $R_{\mathcal{C},\mathcal{C}}$ due to steady cruising were derived by Havelock [8] using a combination of potential flow theory and the method of Fourier transforms. We display these in Appendix A. The wave-field height $h_{\mathcal{C}}$ is plotted in Fig. 2(a) for Froude number Fr = 0.2 [cf. Fig. 1(b) in Ref. [14]]. The famous Kelvin angle [15,16] $\psi = 19.47°$ is indicated with a dashed line. The cruising wave drag $R_{\mathcal{C},\mathcal{C}}$, which is always a negative quantity, is plotted in Fig. 3(a), demonstrating the characteristic extremum at Fr ≈ 0.45. We compare $R_{\mathcal{C},\mathcal{C}}$ with the profile drag R_d (9) in the same plot. Note the change in behavior between $R_{\mathcal{C},\mathcal{C}}$ and R_d that takes place near Fr ≈ 0.3. For Fr > 0.3, a significant part of the drag comes from radiating waves away ($R_{\mathcal{C},\mathcal{C}}$), whereas for Fr < 0.3 this becomes negligible compared to the profile drag (R_d).

B. Waves due to heaving and pitching

Next, we discuss the additional waves generated by heaving and pitching motions. Here we follow an approach inspired by recent studies of bouncing droplets on liquid surfaces and their resultant wave fields [2]. In particular, we assume that the effect of the oscillations (4) and (5) is akin to the effect of a corresponding source term in a linear wave equation for the surface height $h(x, y, t)$. For forcing frequency ω, the dominant component of the resultant wave field has a gravity-based wave number $k = \omega^2/g$, and a gravity-based wave speed $c = g/\omega$. While there may be other
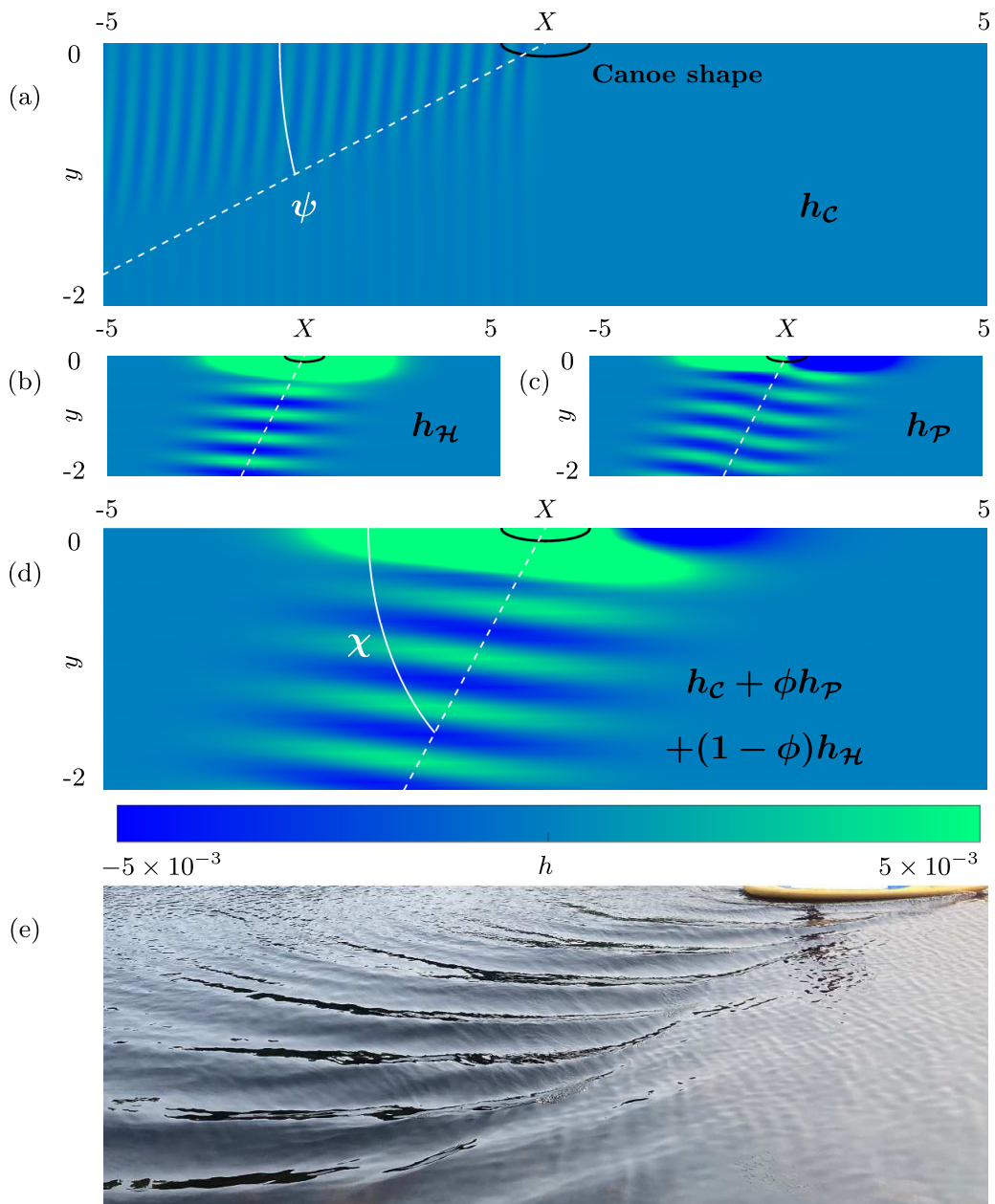
FIG. 2. Wave fields at time $t = 0$ in the case of cruising motion (a), heaving motion (b), pitching motion (c), and the combination of all three (d). Typical parameter values are chosen for the Froude numbers Fr $= 0.2$, $\text{Fr}_\omega = 0.25$, for which the waves due to cruising are very small, so the color scale in (a) is $\times 10^{-5}$. (e) Photo of a typical wave field due to gunwale bobbing (see also video in the Supplemental Material [13]).

dispersive waves present, the predominant waves must travel at this speed and thus satisfy the linear equation

$$\frac{1}{\text{Fr}_\omega^2} \frac{\partial^2 h_n}{\partial t^2} - \nabla^2 h_n = \nabla^2 p_n, \quad n = \mathcal{H}, \mathcal{P}. \tag{12}$$
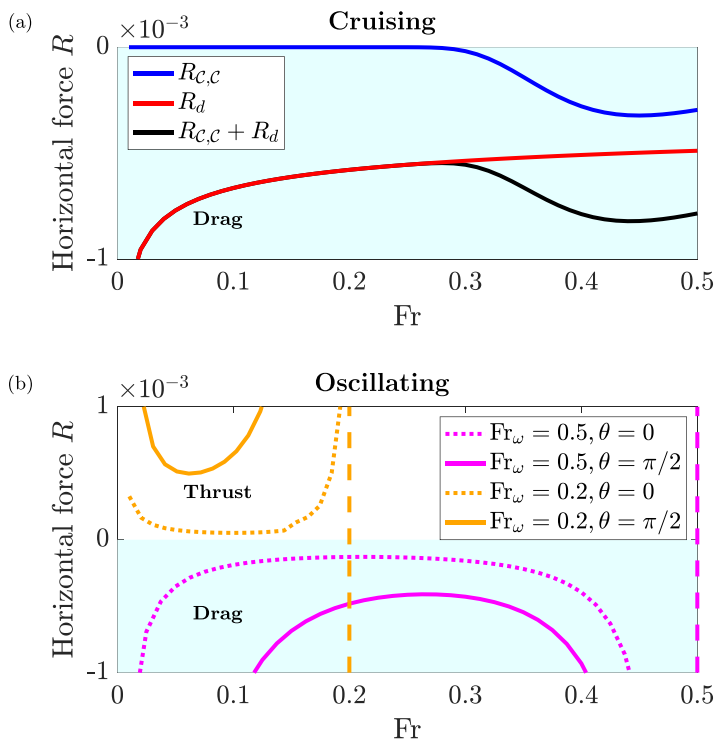
FIG. 3. Horizontal forces due to cruising (a) and oscillating (b). The forces due to cruising $R_{\mathcal{C},\mathcal{C}} + R_d$ are always negative (drag), whereas the summed forces due to oscillating $R_{n,m}$ [see (10)] are either positive (thrust) or negative (drag) depending on the parameters $\mathrm{Fr}_\omega, \theta, \phi, \alpha, \beta$. Mach limits $\mathrm{Ma} = 1$ (13) are indicated with dashed lines.

The oscillating Froude number is proportional to the phase speed, $\mathrm{Fr}_\omega = c/\sqrt{gL}$, illustrating its similarity with the cruising Froude number (1). The Mach number for the flow is given by the ratio

$$\mathrm{Ma} = \mathrm{Fr}/\mathrm{Fr}_\omega = U/c, \tag{13}$$

which must be less than one to avoid shocks.

The oscillating wave fields are calculated using a Lorentz transformation, with a Lorentz factor $\gamma = (1 - U^2/c^2)^{-1/2}$, and Green's functions for the Helmholtz equation [2], the details of which are presented in Appendix B. The wave-field heights are given by

$$h_n = \mathrm{Im}\{\mathrm{Fr}_\omega^2 \gamma^{-1} \bar{h}_n \exp[i\mathrm{Fr}_\omega^{-1} t]\}, \quad n = \mathcal{H}, \mathcal{P}, \tag{14}$$

where $\bar{h}_n$ is the complex wave field given in terms of the integrated pressure source. The wave-field heights (14) for heaving, $h_\mathcal{H}$, and pitching, $h_\mathcal{P}$, are calculated numerically and plotted in Figs. 2(b) and 2(c) for typical parameter values. The canoe acts as a line source, sending waves laterally outwards, predominantly at the Mach angle [17], $\chi = 90° - \tan^{-1}\mathrm{Ma} \approx 51°$. The combined wave field due to heaving and pitching is displayed in Fig. 2(d), showing qualitative resemblance with the waves due to gunwale bobbing in Fig. 2(e).

The corresponding horizontal forces due to heaving and pitching are found by numerically evaluating (8) (see simplifications in Appendix B). The results are plotted in Fig. 3(b) for different values of the Froude number in the range $\mathrm{Fr} \in [0, \mathrm{Fr}_\omega]$, with heaving and pitching either in phase ($\theta = 0$) or out of phase ($\theta = \pi/2$). Unlike the force due to cruising, $R_{\mathcal{C},\mathcal{C}}$, which is always negative, the force due to oscillating (8) may be either negative (drag) or positive (thrust) depending on the
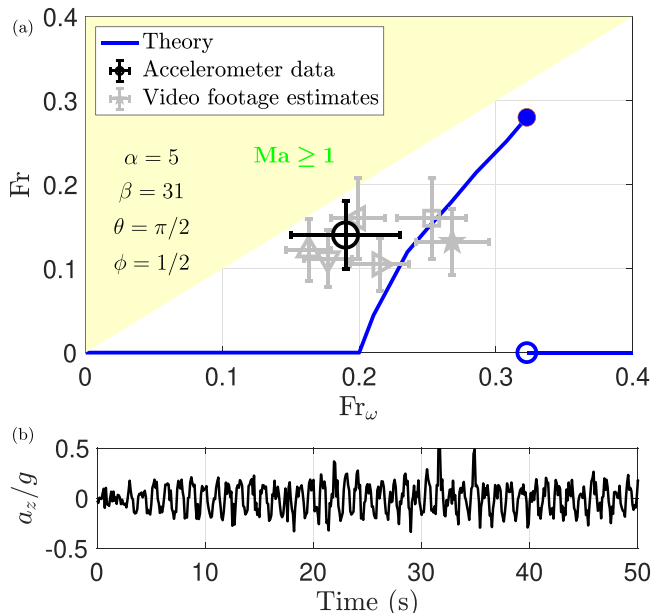
FIG. 4. (a) Solutions to the thrust-drag equation (11), incorporating wave drag (7), profile drag (9), and thrust due to oscillating (8), for different values of the oscillating Froude number Fr_ω. Our experimental data point (calculated using an accelerometer) is plotted as a black circle. Other data points taken from video data of gunwale bobbing on canoes and paddle boards of different shapes and sizes are shown in gray (see Appendix D for more details). (b) A sample of the vertical acceleration divided by g, measured using an accelerometer while gunwale bobbing.

other parameter values. Typically, the largest positive values of (8) are observed for out-of-phase pitch and heave in equal proportion, $\theta \approx \pi/2$, $\phi \approx 1/2$, which appears to match with the motions of successful gunwale bobbing, as discussed below.

IV. GUNWALE BOBBING IN ACTION

When the thrust matches the drag (steady cruising), we can solve the force balance (11) for the cruising Froude number Fr. For typical parameter values, there is either a single unique solution Fr or no solution other than a vanishing speed, as plotted in Fig. 4(a). Our results indicate that gunwale bobbing should be possible for the range $0.2 \leqslant \mathrm{Fr}_\omega \leqslant 0.32$ (with an abrupt cutoff when drag exceeds possible thrust values) and results in a cruising Froude number in the range $0 \leqslant \mathrm{Fr} \leqslant 0.28$. In this regime, profile drag is much larger than wave drag $R_d \gg R_{\mathcal{C},\mathcal{C}}$, so it provides the dominant force to be balanced against the thrust generated by oscillations.

We compare our theoretical results to accelerometer data taken from a gunwale bobber jumping on one end of a canoe of length $L = 4.7\,\mathrm{m}$, width $W = 0.94\,\mathrm{m}$, and draft $D = 0.15\,\mathrm{m}$. In a series of eight trials, the canoe was driven over a distance of 25 m, taking between 20 s and 50 s. The vertical acceleration a_z for one trial is plotted in Fig. 4(b), and the rest are shown in Appendix D. Cruising and oscillating Froude numbers were calculated as $\mathrm{Fr} = 0.14 \pm 0.04$ and $\mathrm{Fr}_\omega = 0.19 \pm 0.04$, which we illustrate with a circular data point in Fig. 4(a). We note that the bobbing frequency is likely to have been close to the natural frequency of the canoe. In Appendix C, we have estimated the natural frequencies for heaving and pitching by approximating the canoe shape with two tetrahedrons, finding $\mathrm{Fr}_\omega \approx 0.42, 0.30$ in each case.

In addition to our canoe, trials were also performed on a smaller paddle board [see Fig. 1(a)]. Although accelerometer data were not collected in this case, we have calculated approximate values

for Fr and Fr$_\omega$ by analyzing frames taken from video footage of the experiment. We have also applied this analysis to video footage of the original canoe, as well as publicly available video footage on the internet for comparison. In this way, additional field data points have been added (in gray) to Fig. 4(a), though direct comparison should be treated with caution, since the aspect ratios of some of these vessels are not the same as our canoe. Further details of the dimensions of the paddle board, and the specific videos used for the video analysis, may be found in Appendix D.

It is unclear whether the forcing used in the experiments corresponds to the model heave and pitch parameters, $\phi = 1/2$, $\theta = \pi/2$. However, agreement between experiment and theory is qualitatively good, though we calculate optimum Froude numbers Fr and Fr$_\omega$ around $2\times$ and $1.7\times$ those of the experimental observations, respectively. It is important to note, however, the many simplifications used in the model such as for the shape of the canoe, the linearity of the waves, the profile drag model, etc. Our model probably captures the physical mechanism behind gunwale bobbing and provides an estimate for the permissible range of parameter values. It cannot, however, provide quantitative predictions at this stage.

To further motivate our assumption that the waves are linear, let us consider the vertical acceleration divided by gravity, a_z/g [see accelerometer data in Figs. 4(b) and 7 below]. This is typically less than around 0.4 across all trials, indicating that the waves are of relatively small amplitude. However, some of our canoe video footage shows waves of significant amplitude, indicating that nonlinear effects may then be present, and as such this could explain why the circular data point in Fig. 4(a) is larger than the theoretical prediction. The waves generated by the paddle board, as seen in Figs. 1(a) and 2(e), are much smaller than for the canoe, and so the linear theory is particularly suitable for this case.

Finally, it is interesting to consider the efficiency of gunwale bobbing, and how this compares with other boat propulsion methods. In the framework of the present model, efficiency is the ratio between propulsive power and total applied power,[2] which is

$$\eta = \frac{\int_0^T \left(\iint_{-\infty}^{+\infty} U p \frac{\partial h}{\partial X} \, dX \, dy \right) dt}{\int_0^T \left(\iint_{-\infty}^{+\infty} \left| p \frac{\partial h}{\partial t} \right| \, dX \, dy \right) dt}. \tag{15}$$

For the theoretical solutions plotted in Fig. 4(a), efficiency is calculated in the range $\eta = 0\%$–17%, with a unique maximum at Fr$_\omega = 0.22$, Fr $= 0.08$. Therefore, while gunwale bobbing appears to be quite an inefficient method of transport, this may explain why the experimental data are located near this value of Fr$_\omega$. Due to the way energy is injected in our model (via pressure applied to the surface), it is difficult to compare efficiency directly with other methods of boat propulsion. Nevertheless, we note that the propulsive efficiency of a rowing oar blade is typically around $\sim 80\%$ [19], and that the efficiency of rowing may be increased further by incorporating a bobbing-type motion.

V. DISCUSSION AND PERSPECTIVES

We have demonstrated, both experimentally and using a simple model based on linear wave theory, that a canoe can be driven forwards by pushing into the surface gradients of the wave field generated by its own forced oscillation. While this study appears to be the first to propose a physical mechanism for gunwale bobbing, numerous other studies have investigated other types of propulsion by waves. For example, Longuet-Higgins [20] demonstrated that a wave generator can be used to drive a boat forward. Meanwhile, Yuan *et al.* [4] have suggested a possible mechanism for wave-induced propulsion when ducklings swim in the wake of their mother. We note that *foil pumping*, a mechanism by which a person can drive a submerged hydrofoil forwards by pumping it with their

---

[2]Note that the integrand for the applied power [i.e., the denominator of (15)] is taken as the absolute value since this is consistent with power measurements in other sports applications [18].

legs, appears to be more similar to swimming than gunwale bobbing, since the propulsion results from the flow around the foil as opposed to the surface wave field.

It is interesting to examine the analogy between the initial transient of gunwale bobbing and the transition to the walking state of a bouncing droplet in a bath of vibrating silicon oil, as described by Moláček and Bush [1]. The bouncing droplets generate a circularly symmetric wave field and only begin to walk following a symmetry-breaking bifurcation. In our theory, by contrast, the fore-aft symmetry is broken by the combination of pitching and heaving, which allows for a finite thrust at zero cruising velocity.

In general, there are several similarities and differences between gunwale bobbing and walking droplets. Both involve thrust generated by interactions with self-generated waves, but the canoe generates traveling waves, while the bouncing droplets excite standing subcritical Faraday waves. The two phenomena occur at vastly different Reynolds numbers. Other similar types of wave-driven particles have been described in the literature, such as the capillary surfers of Ho *et al*. [21]. However, in that study energy is injected externally via a vibrating bath, whereas during gunwale bobbing energy is provided internally by the human on board.

Nevertheless, these comparisons suggest some interesting perspectives. For example, future studies could investigate whether gunwale bobbing exhibits any similarities with the quantum hydrodynamic analogs described by Bush and Oza [22]. In particular, it would be interesting to investigate under what circumstances, if any, the striking similarities that have been observed between walking droplets and Bohmian pilot-wave quantum mechanics can be extended to the case of gunwale bobbing.

In order to gather further experimental data of gunwale bobbing for comparison with this or other studies of wave-driven propulsion, it would be useful to perform some small-scale laboratory experiments. Having attempted to do so ourselves, we found that the chief difficulty lay in striking a balance between choosing an oscillatory motion that is strong enough to excite forward thrust, while being weak enough to not capsize. On this note, it would be interesting to further explore the natural frequencies of the canoe, and whether these can be tuned (by alteration of the shape or mass distribution, say) to make gunwale bobbing *easier*. This would be useful either for conducting small-scale experiments in the laboratory or for making gunwale bobbing more accessible to the novice.

Finally, a potentially important application of this work is to competitive water sports, and in particular rowing [9,23,24]. During rowing races, athletes generate a significant downward force at a frequency of around ∼0.5 Hz each time they generate a stroke. Considering that the length of a singles rowing scull is around ∼8 m [5], this corresponds to an oscillating Froude number of $Fr_\omega \approx 0.35$ (and a cruising speed of $U \approx 5$ m/s, or $Fr \approx 0.56$). Hence, while the main propulsive thrust of a rowing boat comes from the oars, a small contribution may also come from the gunwale bobbing effect. However, it should be noted that the Mach number for such flows is clearly larger than one, indicating the need to extend our model to account for shocks. Nevertheless, our work paves the way forward for future possibilities in optimizing rowing strokes to benefit from boat-wave interactions: At Olympic-level competitions, even fractions of percentages are worth their weight in gold (medals).

ACKNOWLEDGMENTS

APPENDIX A: DERIVATION OF THE WAVE FIELD FOR CRUISING

In this Appendix, we derive expressions for the wave-field height and wave resistance for a cruising canoe, which are based on the linear theory first developed by Havelock [8]. To avoid

following these derivations from first principles (since they are very long), we begin by referencing the main equations for the wave field (in general form) and resistance taken from other literature, and continue thereon. Nevertheless, a full derivation of the theory of wave resistance can be found in [8].

We start with the expression for the wave field, as formulated by Benzaquen *et al.* [7], such that

$$h_{\mathcal{C}} = -\frac{1}{4\pi^2} \lim_{\epsilon \to 0} \iint_0^\infty \frac{\kappa(\mathcal{F}p_{\mathcal{C}})}{\kappa - \mathrm{Fr}^2 k_X^2 + 2i\epsilon k_X} \exp[-i(k_X X + k_y y)] \, dk_X \, dk_y, \tag{A1}$$

where k_X, k_y, are the wave numbers in the X and y directions, $\kappa = (k_X^2 + k_y^2)^{1/2}$ is the wave-number magnitude, ϵ is a dummy asymptotic variable, and $\mathcal{F}p_{\mathcal{C}}$ is the Fourier transform of the cruising pressure disturbance, which is

$$\mathcal{F}p_{\mathcal{C}} = \frac{\delta}{\alpha\beta} \exp\left[-\left(k_X^2 + k_y^2/\alpha^2\right)/4\pi^2\right]. \tag{A2}$$

We write (A1) in a form which is amenable to the Sokhotski-Plemelj theorem from complex analysis, such that

$$h_{\mathcal{C}} = -\frac{\delta}{4\pi^2\alpha\beta} \lim_{\epsilon \to 0} \iint_0^\infty \frac{(\kappa/2k_X)}{(\kappa - \mathrm{Fr}^2 k_X^2)/2k_X + i\epsilon} \exp\left[-i(k_X X + k_y y) - \left(k_X^2 + k_y^2/\alpha^2\right)/4\pi^2\right] dk_X \, dk_y. \tag{A3}$$

By defining the functions

$$A(k_X, k_y) = (\kappa/2k_X) \exp\left[-i\left(k_X X + k_y y\right) - \left(k_X^2 + k_y^2/\alpha^2\right)/4\pi^2\right], \tag{A4}$$

$$B(k_X, k_y) = \left(\kappa - \mathrm{Fr}^2 k_X^2\right)/2k_X, \tag{A5}$$

the integral (A3) can be written (via a change of variables) as

$$h_{\mathcal{C}} = -\frac{\delta}{4\pi^2\alpha\beta} \lim_{\epsilon \to 0} \int_0^\infty \int_\infty^{-\infty} \frac{A(\partial B/\partial k_X)^{-1}}{B + i\epsilon} \, dB \, dk_y. \tag{A6}$$

Hence, upon application of the Sokhotski-Plemelj theorem, this reduces to

$$h_{\mathcal{C}} \approx -\frac{\delta}{4\pi^2\alpha\beta} \int_0^\infty -i\pi A[k_X^*(k_y), k_y]\{\partial B/\partial k_X[k_X^*(k_y), k_y]\}^{-1} \, dk_y, \tag{A7}$$

where k_X^* is the critical wave number for which $B = 0$, which is

$$k_X^* = \mathrm{Fr}^{-2}\left[1/2 + \left(1/4 + \mathrm{Fr}^4 k_y^2\right)^{1/2}\right]^{1/2}. \tag{A8}$$

Note that (A7) ignores a second term in the Sokhotski-Plemelj theorem (proportional to the Cauchy principal value), since it is asymptotically small. The partial derivative of B with respect to k_X in (A7) is evaluated as

$$\partial B/\partial k_X = \frac{1}{2\kappa} - \frac{\kappa}{2k_X^2} - \frac{\mathrm{Fr}^2}{2}, \tag{A9}$$

which, evaluated at the critical wave number is

$$\partial B/\partial k_X[k_X^*(k_y), k_y] = \frac{1}{2\mathrm{Fr}^2[k_X^*(k_y)]^2} - \mathrm{Fr}^2. \tag{A10}$$

Hence, the wave field is ultimately written as

$$h_{\mathcal{C}} = \frac{-i\mathrm{Fr}^2\delta}{4\pi\alpha\beta} \int_0^\infty F[k_X^*(k_y), k_y, X, y] \, dk_y, \tag{A11}$$

with the function

$$F = \frac{\kappa}{k_X(2\mathrm{Fr}^4 - k_X^{-2})} \exp\left[-\frac{1}{4\pi^2\alpha^2}(k_X^2\alpha^2 + k_y^2) - i(k_X X + k_y y)\right]. \tag{A12}$$

The corresponding wave resistance is written (following Benham $et\ al.$ [9], except using an inertial scaling $\rho U^2 L^2$ as the normalization instead of $mg = \rho g L^3/\alpha\beta$) as

$$R_{\mathcal{C},\mathcal{C}} = \frac{\delta^2}{4\mathrm{Fr}^4\alpha^2\beta^2} \int_0^\infty C[k_X^*(k_y), k_y]\{2\mathrm{Fr}^{-2}\,\partial B/\partial k_X[k_X^*(k_y), k_y]\}^{-1}\,dk_y, \tag{A13}$$

with the function

$$C(k_X, k_y) = \kappa \exp\left[-\left(k_X^2 + k_y^2/\alpha^2\right)/2\pi^2\right]. \tag{A14}$$

Hence, the wave resistance simplifies to

$$R_{\mathcal{C},\mathcal{C}} = -\frac{\delta^2}{4\alpha^2\beta^2} \int_0^\infty G[k_X^*(k_y), k_y]\,dk_y, \tag{A15}$$

with the function

$$G = \frac{\kappa}{2\mathrm{Fr}^4 - k_X^{-2}} \exp\left[-\frac{1}{2\pi^2\alpha^2}\left(k_X^2\alpha^2 + k_y^2\right)\right]. \tag{A16}$$

APPENDIX B: DERIVATION OF THE WAVE FIELD FOR OSCILLATING HEAVE OR PITCH

Consider the linear wave equation

$$\mathrm{Fr}_\omega^{-2}\frac{\partial^2 h_n}{\partial t^2} - \nabla^2 h_n = \nabla^2 p_n, \quad n = \mathcal{H}, \mathcal{P}, \tag{B1}$$

with source terms p_n given by (4) and (5). We apply a Lorentz transformation

$$X' = \gamma(x - \mathrm{Fr}\,t) = \gamma X, \tag{B2}$$

$$y' = y, \tag{B3}$$

$$t' = \gamma\left(t - \mathrm{Fr}\mathrm{Fr}_\omega^{-2}x\right) = t/\gamma - \gamma\mathrm{Fr}\mathrm{Fr}_\omega^{-2}X, \tag{B4}$$

where $\gamma = (1 - \mathrm{Fr}^2/\mathrm{Fr}_\omega^2)^{-1/2} = (1 - \mathrm{Ma}^2)^{-1/2}$. Under the transformation (B2)–(B4), the left-hand side of the wave equation (B1) is invariant. Hence, (B1) is rewritten as

$$\mathrm{Fr}_\omega^{-2}\frac{\partial^2 h_n}{\partial t'^2} - \nabla'^2 h_n = \left(\gamma^2\frac{\partial^2}{\partial X'^2} + \frac{\partial^2}{\partial y'^2}\right)p_n\left[X'/\gamma, y', \gamma\left(t' + \mathrm{Fr}\mathrm{Fr}_\omega^{-2}X'\right)\right], \tag{B5}$$

where the original time variable t is replaced using the inverse transformation identity $t = \gamma(t' + \mathrm{Fr}\mathrm{Fr}_\omega^{-2}X')$. By inserting the expressions

$$h_n = \mathrm{Im}\left\{\gamma^{-1}\mathrm{Fr}_\omega^2 h_n^* \exp\left[i\gamma\mathrm{Fr}_\omega^{-1}t'\right]\right\}, \tag{B6}$$

$$p_n = \mathrm{Im}\left\{\gamma\mathrm{Fr}_\omega^{-2} p_n^* \exp\left[i\gamma\mathrm{Fr}_\omega^{-1}t'\right]\right\}, \tag{B7}$$

into (B5), and by rescaling the variables $(\tilde{X}, \tilde{y}) = \gamma\mathrm{Fr}_\omega^{-2}(X', y')$, we arrive at the Helmholtz equation

$$h_n^* + \tilde{\nabla}^2 h_n^* = -\gamma^2\mathrm{Fr}_\omega^{-4}\left(\gamma^2\frac{\partial^2}{\partial\tilde{X}^2} + \frac{\partial^2}{\partial\tilde{y}^2}\right)p_n^*, \tag{B8}$$

where the complex source terms are

$$p_{\mathcal{H}}^* = \frac{\delta \mathrm{Fr}_\omega^2}{\beta \gamma} \exp\left\{-\mathrm{Fr}_\omega^4[\tilde{X}^2 + (\alpha\gamma)^2\tilde{y}^2]/2\gamma^4 + i\mathrm{Ma}\tilde{X}\right\}, \tag{B9}$$

$$p_{\mathcal{P}}^* = \frac{\delta \mathrm{Fr}_\omega^4}{\beta \gamma^3}\tilde{X} \exp\left\{i\theta - \mathrm{Fr}_\omega^4[\tilde{X}^2 + (\alpha\gamma)^2\tilde{y}^2]/2\gamma^4 + i\mathrm{Ma}\tilde{X}\right\}. \tag{B10}$$

As described by Devauchelle *et al.* [2], the solution to (B8) is

$$h_n^* = \frac{i}{4}\iint_{-\infty}^{+\infty} H_0^{(1)}(|\tilde{\mathbf{X}} - \tilde{\boldsymbol{\mathcal{X}}}|)\gamma^2\mathrm{Fr}_\omega^{-4}\left(\gamma^2\frac{\partial^2}{\partial\tilde{\mathcal{X}}^2} + \frac{\partial^2}{\partial\tilde{\mathcal{Y}}^2}\right)p_n^*(\tilde{\boldsymbol{\mathcal{X}}})\,d\tilde{\boldsymbol{\mathcal{X}}}, \tag{B11}$$

written in terms of the Hankel function of the first kind and zeroth order $H_0^{(1)}$ (which is the Green's function for the Helmholtz equation) and integrated over dummy variables $\tilde{\boldsymbol{\mathcal{X}}} = (\tilde{\mathcal{X}}, \tilde{\mathcal{Y}})$. To acquire the final solution for the wave field, we rewrite expressions (B6) and (B7) in terms of the original time variable t, noting that

$$i\mathrm{Fr}_\omega^{-1}\gamma t' = i\mathrm{Fr}_\omega^{-1}t - i\tilde{X}\mathrm{Fr}\mathrm{Fr}_\omega^{-1} = i\mathrm{Fr}_\omega^{-1}t - i\mathrm{Ma}\tilde{X}. \tag{B12}$$

Hence, the wave field and pressure source are given by

$$h_n = \mathrm{Im}\left\{\gamma^{-1}\mathrm{Fr}_\omega^2\bar{h}_n(\tilde{X}, \tilde{y})\exp\left[i\mathrm{Fr}_\omega^{-1}t\right]\right\}, \tag{B13}$$

$$p_n = \mathrm{Im}\left\{\gamma\mathrm{Fr}_\omega^{-2}\bar{p}_n(\tilde{X}, \tilde{y})\exp\left[i\mathrm{Fr}_\omega^{-1}t\right]\right\}, \tag{B14}$$

where

$$\bar{h}_n = h_n^*\exp\left(-i\mathrm{Ma}\tilde{X}\right) = \left[\frac{i}{4}\iint_{-\infty}^{+\infty} H_0^{(1)}(|\tilde{\mathbf{X}} - \tilde{\boldsymbol{\mathcal{X}}}|)\mathcal{L}\bar{p}_n(\tilde{\boldsymbol{\mathcal{X}}})\exp\left(i\mathrm{Ma}\tilde{X}\right)d\tilde{\boldsymbol{\mathcal{X}}}\right]\exp\left(-i\mathrm{Ma}\tilde{X}\right), \tag{B15}$$

$$\bar{p}_n = p_n^*\exp\left(-i\mathrm{Ma}\tilde{X}\right) = \begin{cases} \frac{\delta\mathrm{Fr}_\omega^2}{\beta\gamma}\exp\left\{-\mathrm{Fr}_\omega^4[\tilde{X}^2 + (\alpha\gamma)^2\tilde{y}^2]/2\gamma^4\right\}, & n = \mathcal{H}, \\ \frac{\delta\mathrm{Fr}_\omega^4}{\beta\gamma^3}\tilde{X}\exp\left\{i\theta - \mathrm{Fr}_\omega^4[\tilde{X}^2 + (\alpha\gamma)^2\tilde{y}^2]/2\gamma^4\right\}, & n = \mathcal{P}, \end{cases} \tag{B16}$$

where the operator $\mathcal{L} = \gamma^2\mathrm{Fr}_\omega^{-4}(\gamma^2\partial^2/\partial\tilde{\mathcal{X}}^2 + \partial^2/\partial\tilde{\mathcal{Y}}^2)$. Now, to calculate the force $R_{n,m}$, we start with the expression for the horizontally resolved pressure force

$$R_{n,m} = \frac{1}{\mathrm{Fr}^2 T}\int_0^T\left(\iint_{-\infty}^{+\infty} p_n\frac{\partial h_m}{\partial X}\,dX\,dy\right)dt. \tag{B17}$$

Noting that

$$\frac{\partial h_n}{\partial X} = \mathrm{Im}\left\{\gamma\frac{\partial\bar{h}_n}{\partial\tilde{X}}\exp\left(i\mathrm{Fr}_\omega^{-1}t\right)\right\}, \tag{B18}$$

the force (B17) is given in dimensionless terms as

$$R_{n,m} = \frac{\mathrm{Fr}_\omega^2}{\mathrm{Fr}^2\gamma T}\int_0^T\iint_{-\infty}^{+\infty}\mathrm{Im}\left\{\bar{p}_n\exp\left(i\mathrm{Fr}_\omega^{-1}t\right)\right\}\mathrm{Im}\left\{\frac{\partial\bar{h}_m}{\partial\tilde{X}}\exp\left(i\mathrm{Fr}_\omega^{-1}t\right)\right\}d\tilde{X}\,d\tilde{y}\,dt. \tag{B19}$$

However, we note that for any complex variables A and B which are time-independent, the following simplification can be made:

$$\frac{1}{T}\int_0^T\mathrm{Im}\left\{A\exp\left(i\mathrm{Fr}_\omega^{-1}t\right)\right\}\mathrm{Im}\left\{B\exp\left(i\mathrm{Fr}_\omega^{-1}t\right)\right\}dt = \frac{1}{2}[\mathrm{Im}\{A\}\mathrm{Im}\{B\} + \mathrm{Re}\{A\}\mathrm{Re}\{B\}]. \tag{B20}$$
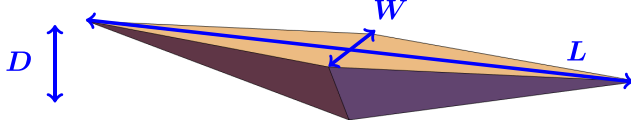
FIG. 5. Canoe shape approximated by two tetrahedrons with total length, width, and draft, L, W, and D, respectively.

In this way, (B19) can be simplified to give

$$R_{n,m} = \frac{\mathrm{Fr}_\omega^2}{2\mathrm{Fr}^2\gamma} \iint_{-\infty}^{+\infty} \left(\mathrm{Re}\,\bar{p}_n \, \mathrm{Re}\,\frac{\partial \bar{h}_m}{\partial \tilde{X}} + \mathrm{Im}\,\bar{p}_n \, \mathrm{Im}\,\frac{\partial \bar{h}_m}{\partial \tilde{X}} \right) d\tilde{X}\,d\tilde{y}. \tag{B21}$$

APPENDIX C: CANOE SURFACE AREA AND NATURAL FREQUENCIES

We approximate the surface area of the canoe by considering two tetrahedrons stuck together with the same total dimensions, as illustrated in Fig. 5. The wetted area of one of the exposed triangles of the tetrahedron surface can be calculated through trigonometry, giving

$$A = \tfrac{1}{8}[L^2W^2 + 4D^2(L^2 + W^2)]^{1/2}. \tag{C1}$$

Hence, in dimensionless coordinates, the total surface area (four triangles) is

$$\mathcal{S} = \left[\frac{1}{4\alpha^2} + \frac{1}{\beta^2}\left(1 + \frac{1}{\alpha^2}\right) \right]^{1/2}. \tag{C2}$$

Next, we use this approximate canoe shape to estimate the natural frequencies for heaving and pitching. This is done by considering the simple harmonic motion of small perturbations to the vertical position of the center of mass and pitch angle. To calculate these natural frequencies it is assumed that the canoe is not cruising, such that $\mathrm{Fr} = 0$, $U = 0$. While all of the analysis in this study has so far remained dimensionless, we keep the subsequent analysis dimensional for convenience. To make this clear we have capitalized many variables so as not to be confused with their dimensionless counterparts in the paper. The two variables for which this does not apply are x and t, whose capitals already have prescribed definitions in the paper, so we replace these with hatted capitals, $\hat{X}$, $\hat{T}$, for clarity.

Let the vertical position of the center of mass (measured from the water line) and the pitch angle of the canoe be denoted by $Z(\hat{T})$ and $\varphi(\hat{T})$, respectively. The equations of motion for each of these are given by conservation of linear and angular momentum in the heave and pitch directions, such that

$$(m + m_a)\ddot{Z} = -\iint_S (P - P_a)(\hat{\mathbf{n}} \cdot \hat{\boldsymbol{k}})\,dS - mg, \tag{C3}$$

$$(I + I_a)\ddot{\varphi} = \iint_S (P - P_a)(\mathbf{r} \times \hat{\mathbf{n}}) \cdot \hat{\boldsymbol{j}}\,dS, \tag{C4}$$

where P_a is atmospheric pressure, $\mathbf{r}$ is the position vector measured from the origin, $\hat{\mathbf{n}}$ is the outward pointing unit normal vector to the hull surface (where $S = L^2\mathcal{S}$), m is the mass of the canoe, m_a and I_a are the linear and angular added masses in the heave and pitch directions [25], and I is the moment of inertia, which is defined as

$$I = \rho_0 \iiint_V |\mathbf{r}|^2\,dV, \tag{C5}$$

in terms of the hull material density ρ_0 (assumed constant), and volume V. For simplicity we have ignored the presence of a gunwale bobber in (C5), and instead we have assumed that the mass of the canoe is distributed uniformly over its hull.

We first consider the case of pure heaving ($\varphi = 0$, $Z = Z(\hat{T})$) and attempt to find an approximate expression for the natural frequency. In this case, the center of mass is perturbed vertically according to

$$Z = Z_0 + \zeta(\hat{T}), \tag{C6}$$

where Z_0 is a constant and $|\zeta/Z_0| \ll 1$. Likewise, if $Z = -\Gamma(\hat{X}, Y)$ is the shape function of the canoe composed of two tetrahedrons, then this is also perturbed by $Z = -\Gamma(\hat{X}, Y) + \zeta(\hat{T})$. Since the oscillations are of small amplitude, the pressure on the hull surface is approximately hydrostatic:

$$P \approx P_a - \rho g(-\Gamma + \zeta). \tag{C7}$$

Hence, the leading-order and first-order terms of (C3) reduce to

$$0 = -\rho g \iint_S (\hat{\mathbf{n}} \cdot \hat{\mathbf{k}}) \Gamma \, dS - mg, \tag{C8}$$

$$(m + m_a)\ddot{\zeta} = \left[\rho g \iint_S (\hat{\mathbf{n}} \cdot \hat{\mathbf{k}}) \, dS \right] \zeta, \tag{C9}$$

the first of which sets the mass of the boat and the second of which determines the perturbation dynamics. These are neatly rearranged to give a simple harmonic oscillator equation for the small perturbation, such that

$$\ddot{\zeta} + \omega^2 \zeta = 0, \tag{C10}$$

where the natural frequency is

$$\omega^2 = \frac{g \iint_S (\hat{\mathbf{n}} \cdot \hat{\mathbf{k}}) \, dS}{\iint_S (\hat{\mathbf{n}} \cdot \hat{\mathbf{k}}) \Gamma \, dS (1 + m_a/m)}. \tag{C11}$$

The added mass ratio m_a/m for the tetrahedron shape is unknown, so instead (as a very approximate estimate) we use the value for a heaving ellipse with the same length-depth aspect ratio (see Ref. [26]), which is

$$\frac{m_a}{m} = \frac{\pi \rho L^2/4}{\pi \rho L D/2} = \frac{\beta}{2}. \tag{C12}$$

Due to the symmetries of the tetrahedra, it suffices to consider just one of the outer triangular faces to calculate (C11). Taking Γ as the planar outer face

$$\Gamma = D\left[1 + \frac{2\hat{X}}{L} + \frac{2Y}{W} \right], \tag{C13}$$

which is defined in the range $Y \in [-W(1/2 + \hat{X}/L), 0]$, $\hat{X} \in [-L/2, 0]$, we calculate

$$\hat{\mathbf{n}} \cdot \hat{\mathbf{k}} = -\left[1 + \frac{4}{\beta^2}(1 + \alpha^2) \right]^{-1/2} = -\frac{1}{2\alpha \mathcal{S}(\alpha, \beta)}, \tag{C14}$$

which is a constant. Now the natural heaving frequency ω may be calculated by evaluating the integrals in (C11). After simplification and rewriting in terms of the oscillating Froude number, this provides the result

$$\text{Fr}_\omega = \frac{1}{\omega}\left(\frac{g}{L}\right)^{1/2} = \left(\frac{1 + \beta/2}{3\beta}\right)^{1/2}. \tag{C15}$$

Next we repeat the above analysis for the case of pure pitching ($\zeta = 0$, $\varphi = \varphi(\hat{T})$), centered about the origin. A small perturbation $\varphi \ll 1$ is applied to the pitch angle of the boat, causing the vertical position of the hull to be moved to $Z \approx -\Gamma + \varphi\hat{X}$. To evaluate the right-hand side of (C4), we need to calculate the cross product of the radial vector with the pressure force vector. Each of these vectors is given by

$$\mathbf{r} = \{\hat{X}, Y, -\Gamma + \varphi\hat{X}\}, \tag{C16}$$

$$(P - P_a)\hat{\mathbf{n}} = \frac{-\rho g(-\Gamma + \varphi\hat{X})}{\left[\left(-\frac{\partial\Gamma}{\partial\hat{X}} + \varphi\right)^2 + \frac{\partial\Gamma}{\partial Y}^2 + 1\right]^{1/2}} \left\{-\frac{\partial\Gamma}{\partial\hat{X}} + \varphi, -\frac{\partial\Gamma}{\partial Y}, -1\right\}. \tag{C17}$$

Next we perform the cross product, expand out the variables in powers of φ, and integrate over the surface area of the hull (note that all antisymmetric terms vanish upon integration), ignoring terms of order $O(\varphi^2)$. This gives the result

$$\iint_S (P - P_a)(\mathbf{r} \times \hat{\mathbf{n}}) \cdot \hat{\jmath} \, dS$$

$$\approx -\left[\rho g \iint_S \frac{\hat{X}^2\left(1 + \frac{\partial\Gamma}{\partial\hat{X}}^2 + \frac{\partial\Gamma}{\partial Y}^2\right) + \Gamma^2\left(1 + \frac{\partial\Gamma}{\partial Y}^2\right) + \hat{X}\Gamma\frac{\partial\Gamma}{\partial\hat{X}}\left(1 + 2\frac{\partial\Gamma}{\partial\hat{X}}^2 + 2\frac{\partial\Gamma}{\partial Y}^2\right)}{\left[\frac{\partial\Gamma}{\partial\hat{X}}^2 + \frac{\partial\Gamma}{\partial Y}^2 + 1\right]^{3/2}} \, dS\right]\varphi. \tag{C18}$$

The next step is to calculate the moment of inertia in (C4). To do so we assume that the hull mass is distributed over a thin solid shell of vertical thickness $H \ll \Gamma$, such that the volume element is approximately $dV \approx H dS$ and the hull density $\rho_0 = m/HS$. Hence, the moment of inertia (C5) is given by

$$I \approx \frac{m}{S} \iint_S (\hat{X}^2 + Y^2 + \Gamma^2) \, dS. \tag{C19}$$

Note that only leading-order terms are kept in (C19) since the left-hand side of (C4) is already of order $O(\varphi)$. Using (C8) to replace m (at leading order) with an expression for the mass, then (C19) becomes

$$I \approx \frac{\rho}{S} \iint_S (\hat{X}^2 + Y^2 + \Gamma^2) \, dS \iint_S -(\hat{\mathbf{n}} \cdot \hat{\boldsymbol{k}})\Gamma \, dS. \tag{C20}$$

Hence, the equation of motion (C4) reduces to a simple harmonic oscillator of the form

$$\ddot{\varphi} + \omega^2\varphi = 0, \tag{C21}$$

where

$$\omega^2 =$$

$$\frac{gS \iint_S \left[\hat{X}^2\left(1 + \frac{\partial\Gamma}{\partial\hat{X}}^2 + \frac{\partial\Gamma}{\partial Y}^2\right) + \Gamma^2\left(1 + \frac{\partial\Gamma}{\partial Y}^2\right) + \hat{X}\Gamma\frac{\partial\Gamma}{\partial\hat{X}}\left(1 + 2\frac{\partial\Gamma}{\partial\hat{X}}^2 + 2\frac{\partial\Gamma}{\partial Y}^2\right)\right]\left[\frac{\partial\Gamma}{\partial\hat{X}}^2 + \frac{\partial\Gamma}{\partial Y}^2 + 1\right]^{-3/2} dS}{\iint_S (\hat{X}^2 + Y^2 + \Gamma^2) \, dS \iint_S -(\hat{\mathbf{n}} \cdot \hat{\boldsymbol{k}})\Gamma \, dS(1 + I_a/I)}. \tag{C22}$$

Since the angular added mass ratio I_a/I is unknown for the tetrahedron shape, we use the value for an ellipse with the same length-depth aspect ratio as a very approximate estimate, which is

$$\frac{I_a}{I} = \frac{1/8\pi\rho(L^2/4 - D^2)^2}{1/8\pi\rho LD(L^2/4 + D^2)} = \frac{(\beta^2 - 4)^2}{4\beta(\beta^2 + 4)}. \tag{C23}$$

As before, we exploit the symmetry of the tetrahedra to evaluate the integrals in (C22) by considering only one of the outer triangular faces of the surface (C13). In this way the the natural
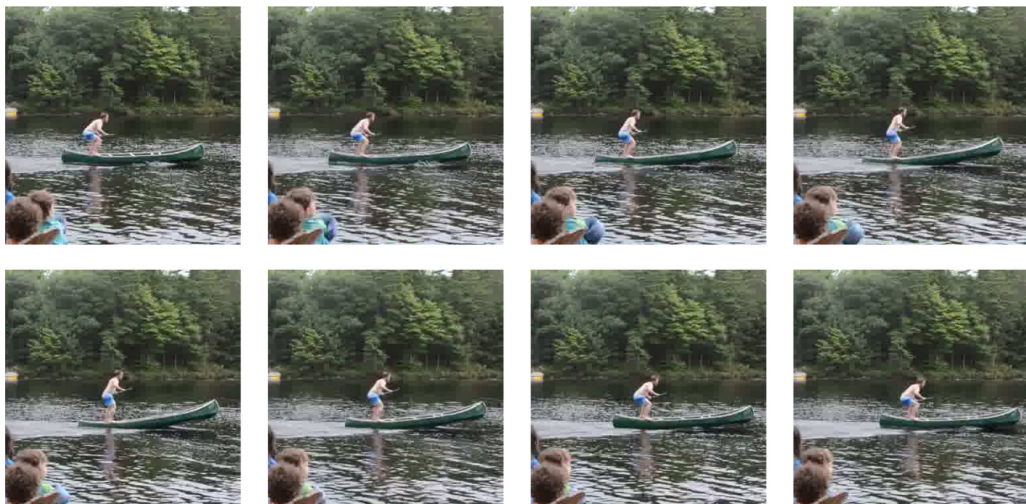
FIG. 6. Photographs of J.A.N. gunwale bobbing on his canoe of dimensions $L, W, D = 4.7, 0.94, 0.15\,\mathrm{m}$, taken at intervals of 0.1 s.

frequency for pitching may be calculated analytically, and we write this (after simplification) in terms of the oscillating Froude number, which is

$$\mathrm{Fr}_\omega = \left[\frac{(4 + 4\alpha^2 + \beta^2)^{1/2}[\beta^2 + \alpha^2(4 + \beta^2)]}{3\alpha^2[-16 + (6 + 4\alpha^2)\beta^2 + \beta^4]} \left(1 + \frac{(\beta^2 - 4)^2}{4\beta(\beta^2 + 4)} \right) \right]^{1/2}. \tag{C24}$$

Hence, inserting $\alpha = 5$, $\beta = 31$, into the (very approximate) expressions for the natural oscillating Froude number (C15) and (C24), we calculate $\mathrm{Fr}_\omega = 0.42$ in the case of heaving and $\mathrm{Fr}_\omega = 0.30$ in the case of pitching.

APPENDIX D: ACCELEROMETER AND VIDEO DATA

The gunwale bobbing experiments were performed by J.A.N. and Miles Neufeld on Muldrew Lake in Ontario, Canada, in August 2021. The accelerometer data used in our study were taken by J.A.N. using the *Accelerometer* app on an iPhone 7 while bobbing on a canoe of dimensions $L, W, D = 4.7, 0.94, 0.15\,\mathrm{m}$. The photographs in Figs. 1(a) and 2(e) corresponded to gunwale bobbing performed by Miles Neufeld on a paddle board of dimensions $L, W, D = 3.05, 0.76, 0.10\,\mathrm{m}$. Photographs of J.A.N. on his canoe are illustrated here in Fig. 6, and a video is uploaded as a separate file [13].

Data for the vertical acceleration during gunwale bobbing over five different trials are plotted in Fig. 7. Aside from the trials corresponding to the displayed accelerometer data, a total eight further gunwale bobbing trials were performed by J.A.N. over a measured distance of 24.73 m between two jetties on the lake to measure the speed of the canoe. The times to complete this journey were $t = 21.5, 21.1, 24.66, 32.98, 29.15, 47.53, 21.41, 20.4$ s. Hence, the average speed plus or minus one standard deviation was $U = 0.97 \pm 0.24$ m/s. It should be noted that the particularly long times of 32.98 s and 47.53 s were the results of trying to gunwale bob at a higher than normal frequency, resulting in particularly suboptimal results.

We have also collected velocity and frequency data by analyzing our own video footage as well as publicly available video footage on the internet. The frequency was estimated by counting the number of oscillations over the length of the video clip, and the velocity was estimated by calculating the number of oscillations needed to traverse the length of the vessel L. In this way a
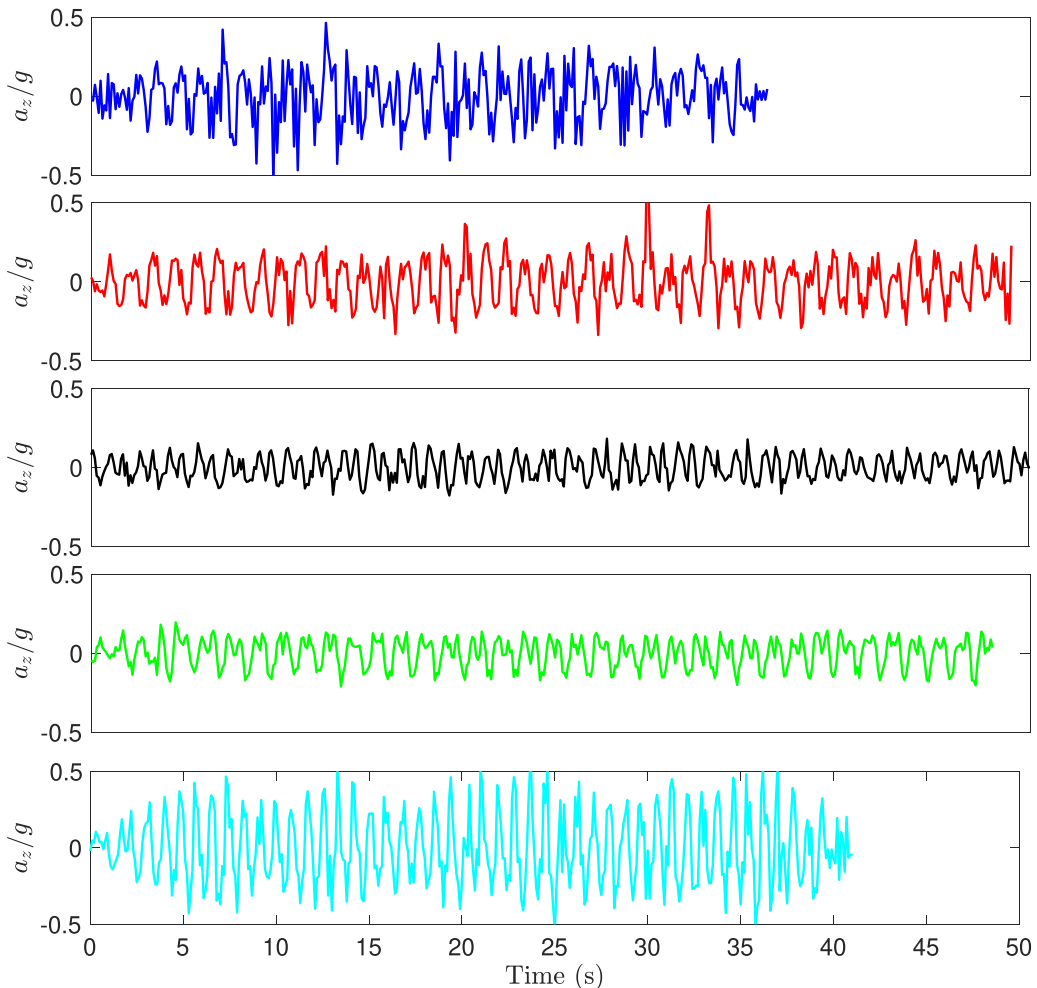
FIG. 7. Experimental data for the vertical acceleration (normalized by g) measured using an accelerometer over five separate trials.

total of six additional data points have been added to Fig. 4(a), where we have taken broad error estimates of $\pm 30\%$ for the velocity and $\pm 10\%$ for the frequency (the velocity is much harder to estimate).

The left and right triangles ($\triangleleft$ and $\triangleright$) correspond to video data of J.A.N. on his canoe, whereas the up and down triangles ($\triangle$ and $\triangledown$) correspond to video data of Miles Neufeld on his paddle board. Square and star symbols ($\square$ and $\star$) correspond to publicly available video data on YouTube, found at the Ref. [27].

APPENDIX E: MODELING PROFILE DRAG

In this Appendix we briefly describe how we model profile drag, which is given by (9). As described by [5], there is a significant contribution to the drag on a canoe from viscous friction at the wetted surface, and from the form drag due to vortex shedding. The skin and form drag are summed together and modeled with a combined profile drag term R_d, given in terms of the dimensionless wetted surface area $\mathcal{S}$ and a drag coefficient C_d [see (9)]. Following [5], the drag

coefficient is approximated by the empirical relationship

$$C_d = C_f(1 + 2/\alpha + 60/\alpha^4), \tag{E1}$$

where C_f is the skin friction coefficient for a flat plate [10]. This varies weakly with the Reynolds number $\mathrm{Re} = UL/\nu$, where ν is the kinematic viscosity, and is approximated for turbulent flows [11] as

$$C_f = 0.075(\log \mathrm{Re} - 2)^{-2}. \tag{E2}$$

For example, a 4.7 m canoe cruising at 1 m/s in water corresponds to a Reynolds number of 4.7×10^6, producing a skin friction value $C_f = 3.4 \times 10^{-3}$.

---

[1] J. Moláček and J. W. M. Bush, Drops bouncing on a vibrating bath, J. Fluid Mech. **727**, 582 (2013).

[2] O. Devauchelle, É. Lajeunesse, F. James, C. Josserand, and P. Y. Lagrée, Walkers in a wave field with memory, CR Mécanique **348**, 591 (2020).

[3] A. Andersen, J. Madsen, C. Reichelt, S. Rosenlund Ahl, B. Lautrup, C. Ellegaard, M. T. Levinsen, and T. Bohr, Double-slit experiment with single wave-driven particles and its relation to quantum mechanics, Phys. Rev. E **92**, 013006 (2015).

[4] Z. M. Yuan, M. Chen, L. Jia, C. Ji, and A. Incecik, Wave-riding and wave-passing by ducklings in formation swimming, J. Fluid Mech. **928**, R2 (2021).

[5] J. P. Boucher, R. Labbé, C. Clanet, and M. Benzaquen, Thin or bulky: Optimal aspect ratios for ship hulls, Phys. Rev. Fluids **3**, 074802 (2018).

[6] M. Benzaquen, F. Chevy, and É. Raphaël, Wave resistance for capillary gravity waves: Finite-size effects, Europhys. Lett. **96**, 34003 (2011).

[7] M. Benzaquen, A. Darmon, and E. Raphaël, Wake pattern and wave resistance for anisotropic moving disturbances, Phys. Fluids **26**, 092106 (2014).

[8] T. H. Havelock, Wave resistance: Some cases of three-dimensional fluid motion, Proc. R. Soc. A **95**, 354 (1919).

[9] G. P. Benham, R. Bendimerad, M. Benzaquen, and C. Clanet, Hysteretic wave drag in shallow water, Phys. Rev. Fluids **5**, 064803 (2020).

[10] S. F. Hoerner, *Fluid-Dynamic Drag: Practical Information on Aerodynamic Drag and Hydrodynamic Resistance* (Hoerner Fluid Dynamics, New York, 1965).

[11] J. B. Hadler, Coefficients for international towing tank conference 1957 model-ship correlation line, Tech. Rep., David Taylor Model Basin, Washington, DC (1958).

[12] G. P. Benham, J. P. Boucher, R. Labbé, M. Benzaquen, and C. Clanet, Wave drag on asymmetric bodies, J. Fluid Mech. **878**, 147 (2019).

[13] See Supplemental Material at http://link.aps.org/supplemental/10.1103/PhysRevFluids.7.074804 for video footage of J.A.N. and Miles Neufeld gunwale bobbing on a canoe and a paddle board.

[14] R. Pethiyagoda, T. J. Moroney, C. J. Lustri, and S. W. McCue, Kelvin wake pattern at small Froude numbers, J. Fluid Mech. **915**, A126 (2021).

[15] W. Thomson (Lord Kelvin), On ship waves, Proc. Inst. Mech. Eng. **38**, 409 (1887).

[16] M. Rabaud and F. Moisy, Ship Wakes: Kelvin or Mach Angle? Phys. Rev. Lett. **110**, 214503 (2013).

[17] H. Ockendon and J. R. Ockendon, *Waves and Compressible Flow* (Springer, New York, 2004).

[18] C. V. Bouten, K. R. Westerterp, M. Verduin, and J. D. Janssen, Assessment of energy expenditure for physical activity using a triaxial accelerometer, Med. Sci. Sports Exerc. **26**, 1516 (1994).

[19] A. Sliasas and S. Tullis, A hydrodynamics-based model of a rowing stroke simulating effects of drag and lift on oar blade efficiency for various cant angles, Proc. Eng. **2**, 2857 (2010).

[20] M. S. Longuet-Higgins, The mean forces exerted by waves on floating or submerged bodies with applications to sand bars and wave power machines, Proc. R. Soc. A. **352**, 463 (1977).

[21] I. Ho, G. Pucci, A. U. Oza, and D. M. Harris, Capillary surfers: Wave-driven particles at a fluid interface, arXiv:2102.11694.

[22] J. W. M. Bush and A. U. Oza, Hydrodynamic quantum analogs, Rep. Prog. Phys. **84**, 017001 (2021).

[23] J. P. Boucher, R. Labbé, and C. Clanet, Row bots, Phys. Today **70**, 82 (2017).

[24] L. Gierczak-Galle, A. Fadle, M. Arutkin, E. Raphael, and M. Benzaquen, Unsteady wave drag on a disturbance moving along an arbitrary trajectory, arXiv:2005.00857.

[25] F. Ursell, On the heaving motion of a circular cylinder on the surface of a fluid, Q. J. Mech. Appl. Math. **2**, 218 (1949).

[26] J. N. Newman, *Marine Hydrodynamics* (MIT Press, Cambridge, MA, 2018).

[27] https://www.youtube.com/watch?v=55IUQKrK0zA, https://www.youtube.com/watch?v=T9Wpm6pxnr0.